Langmuir

Article

pubs.acs.org/Langmuir

Adsorption Mechanism of Myelin Basic Protein on Model Substrates and Its Bridging Interaction between the Two Surfaces

Dong Woog Lee,[†] Xavier Banquy,[‡] Kai Kristiansen,[†] Younjin Min,[§] Arun Ramachandran,[∥] Joan M. Boggs,[⊥,#] and Jacob N. Israelachvili*[,†,▽]

[†]Department of Chemical Engineering, University of California at Santa Barbara, Santa Barbara, California 93106, United States

[‡]Canada Research Chair in Bio-inspired Materials and Interfaces, Faculty of Pharmacy, Université de Montréal C.P. 6128, succursale Centre Ville, Montréal, Québec H3C 3J7, Canada

[§]Department of Polymer Engineering, University of Akron, Akron, Ohio United States

[∥]Department of Chemical Engineering and Applied Chemistry, University of Toronto, 200 College Street, Toronto, Ontario M5S 3E5, Canada

[⊥]Department of Molecular Structure and Function, The Hospital for Sick Children, Toronto, Ontario M5G 1X8, Canada

[#]Department of Laboratory Medicine and Pathobiology, University of Toronto, Toronto, Ontario M5G 1L5, Canada

[▽]Materials Department, University of California, Santa Barbara, California 93106, United States

Supporting Information

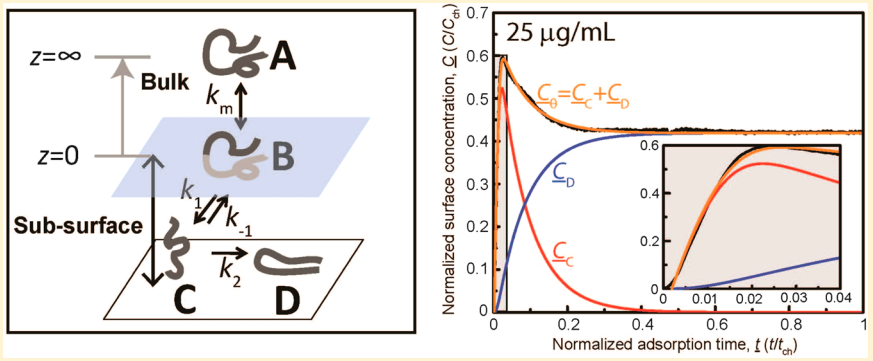

ABSTRACT: Myelin basic protein (MBP) is an intrinsically disordered (unstructured) protein known to play an important role in the stability of myelin's multilamellar membrane structure in the central nervous system. The adsorption of MBP and its capacity to interact with and bridge solid substrates has been studied using a surface forces apparatus (SFA) and a quartz crystal microbalance with dissipation (QCM-D). Adsorption experiments show that MBP molecules adsorb to the surfaces in a swollen state before undergoing a conformational change into a more compact structure with a thickness of ∼3 nm. Moreover, this compact structure is able to interact with nearby mica surfaces to form adhesive bridges. The measured adhesion force (energy) between two bridged surfaces is 1.0 ± 0.1 mN/m, (E_{ad} = 0.21 ± 0.02 mJ/m^2), which is slightly smaller than our previously reported adhesion force of 1.7 mN/m (E_{ad} = 0.36 mJ/m^2) for MBP adsorbed on two supported lipid bilayers (Lee et al., *Proc. Natl. Acad. Sci. U.S.A.* **2014**, *111*, E768−E775). The saturated surface concentration of compact MBP on a single SiO_2 surface reaches a stable value of 310 ± 10 ng/cm^2 regardless of the bulk MBP concentration. A kinetic three-step adsorption model was developed that accurately fits the adsorption data. The developed model is a general model, not limited to intrinsically disordered proteins, that can be extended to the adsorption of various chemical compounds that undergo chemical reactions and/or conformational changes upon adsorbing to surfaces. Taken together with our previously published data (Lee et al., *Proc. Natl. Acad. Sci. U.S.A.* **2014**, *111*, E768−E775), the present results confirm that conformational changes of MBP upon adsorption are a key for strong adhesion, and that such conformational changes are strongly dependent on the nature of the surfaces.

INTRODUCTION

Myelin basic protein (MBP) is an essential protein for stability of the myelin sheath.[1−3] MBP is one of the major proteins (20% of proteins) found in the myelin sheath that surrounds the axons of the central nervous system (CNS). The myelin sheath is a compact stack of lipid bilayers that alternate between cytoplasmic and extracellular leaflets in the radial direction (see Figure 1). MBP acts as a protein glue that bridges and compacts the cytoplasmic leaflets of myelin. Healthy myelin exhibits a very compact structure with a thin water gap distance (∼3−4

Received: January 14, 2015
Revised: February 20, 2015
Published: February 23, 2015

DOI: 10.1021/acs.langmuir.5b00145
Langmuir 2015, 31, 3159−3166

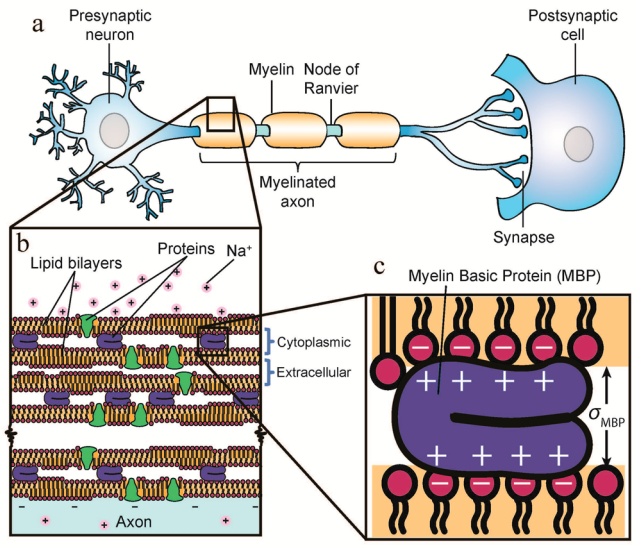

Figure 1. Schematics of the (a) nervous system, (b) myelin, and (c) myelin basic protein (MBP). For illustrative purposes, the intermembrane separation of the cytoplasmic space appears larger than the extracellular space. However, the extracellular space is actually larger than the cytoplasmic space.

nm) between bilayers of the cytoplasmic side, providing a low dielectric constant through the compact bilayers, which in turn allows the axon to transmit electrical impulses in a more efficient and faster manner compared to demyelinated axons.[1−6] Structural changes in the myelin sheath, such as water gap swelling, vacuolization, vesiculation, lesion formation, and delamination are indications of neurological disorders.[7−9] Such neurological disorders are usually embodied by a wide spectrum of symptoms including physical and cognitive disabilities, with multiple sclerosis (MS) being the most common disorder.[6−8]

Myelin basic protein belongs to a family of intrinsically unstructured (disordered) proteins,[10−13] with a predominant isoform named C1 with a molecular weight of 18.5 kDa and a net positive charge of 19.[14] Previous studies conducted with model and extracted bilayers[15−20] have shown that MBP can bind to a negatively charged bilayer via electrostatic and hydrophobic interactions. Recent studies have shown that minute changes in lipid composition lead to changes in lipid domains,[21] where the structure and size of these domains significantly affects the MBP adsorption mechanism, eventually leading to swelling and loss of adhesion between myelin layers.[22]

Structural studies on MBP with circular dichroism (CD) spectroscopy have shown that no structural order exists in the protein when in solution.[3,10] Electron microscopy[16] and solid-state NMR (SSNMR)[23] studies have found that MBP bound to lipid monolayers exhibits a C-shape or hairpin-like structure. However, no study has been performed on the kinetics of MBP adsorption while simultaneously monitoring the changes in conformation of MBP after adsorption to a surface. This study aims to establish a kinetic model that will explain the adsorption and conformational changes of MBP onto a model surface, and how the conformation affects the bridging interaction between the surfaces. In order to measure the bridging force between model surfaces, a surface forces apparatus (SFA) is used. A quartz crystal microbalance with dissipation (QCM-D) was used to measure the adsorption of MBP to SiO_2 surfaces as a function of adsorption time and bulk MBP concentration. A 3-step adsorption model was derived to explain the detailed kinetic information obtained from the QCM-D.

MATERIALS AND METHODS

Materials. The C1 isoform of myelin basic protein was isolated from bovine brain white matter[24] and kept in a deep freezer (−50 °C) until use. MBP was dissolved in buffer (pH 7.4) composed of 150 mM sodium nitrate (Sigma-Aldrich, Inc. *ReagentPlus* ≥ 99%), 10 mM Mops

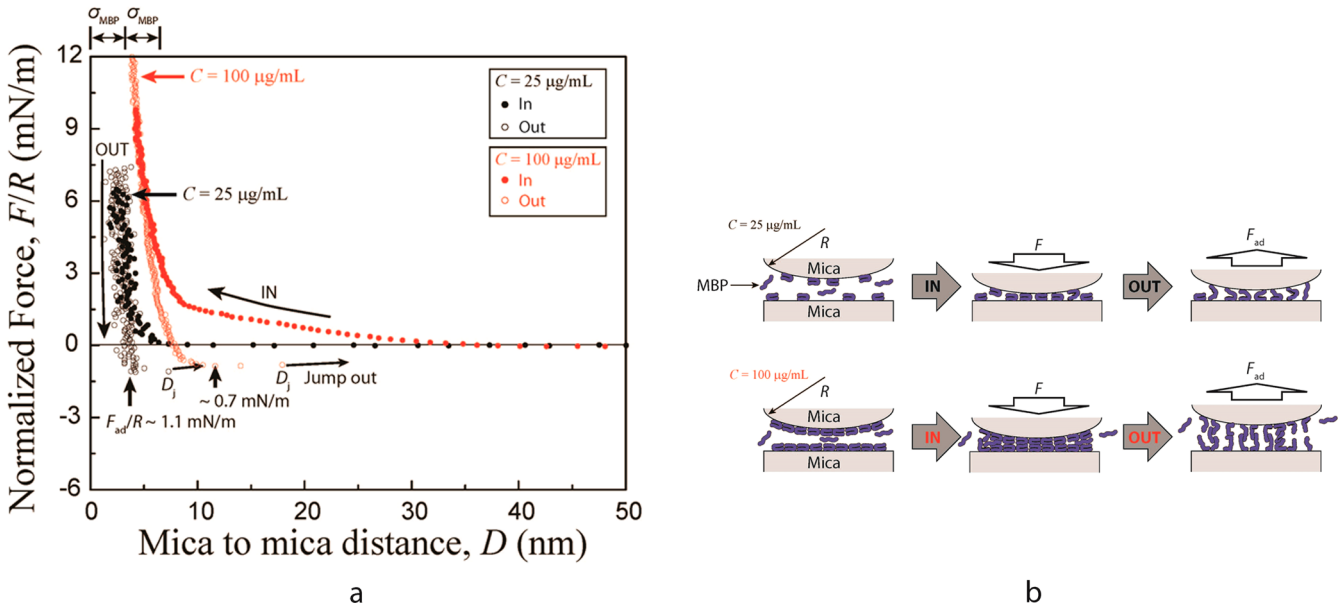

Figure 2. (a) Force−distance (F−D) profiles of MBP between two mica surfaces at two difference concentrations of 25 and 100 μg/mL after 3 h equilibration (3 h after injecting MBP solution between the surfaces), and (b) the schematics showing the possible structuring of MBP during the force runs.

DOI: 10.1021/acs.langmuir.5b00145
Langmuir 2015, 31, 3159−3166

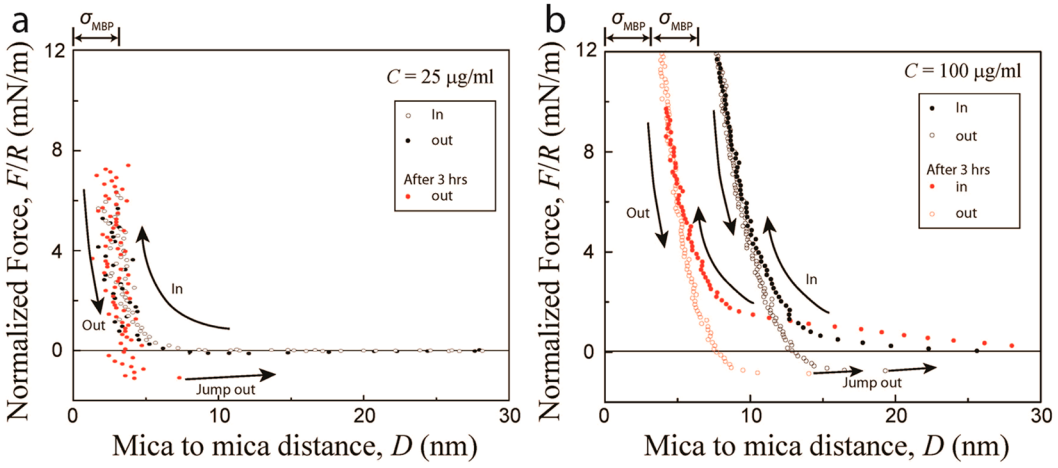

Figure 3. Normalized force−distance (F/R−D) profiles of myelin basic protein (MBP) between two mica surfaces with MBP concentrations of (a) 25 and (b) 100 μg/mL. Initial force runs were performed 15 min after the MBP injection (black circles), followed by another force run after ∼3 h of waiting time (red circles). The force runs after 3 h are the same data as in Figure 2a.

sodium salt (Sigma-Aldrich, Inc. ≥ 99.5%), and 2 mM calcium nitrate tetrahydrate (Sigma-Aldrich, Inc. ≥ 99%) to make a desired concentration of MBP solution. Aliquots of MBP solutions were kept frozen (−50 °C) in acid-cleaned vials until use.

Methods. *SFA Experiments.* An SFA 2000 (SurForce, LLC) was used for the force measurements.[25] Freshly cleaved and back-silvered mica sheets were glued onto two cylindrical disks with curvature radii (R) of ∼2 cm. The surfaces were mounted in the SFA in a cross-cylindrical geometry, which is mathematically equivalent to a sphere-on-flat geometry (see Figure 2b). The separation distance between two surfaces was measured using optical interferometry,[26] and the forces between the two surfaces was measured using a double cantilever spring holding the lower disk. MBP solution was injected between the surfaces, followed by a 15 min equilibration time. For the force-distance measurements, the lower surface was advanced toward the upper surface using a fine-control motorized micrometer with an approach velocity of 0.5−1.0 nm/s, followed by separation of the two surfaces at the same velocity, in order to measure the adhesion force. After the first force run, MBP was allowed to further and completely adsorb and equilibrate on the surfaces for 3 h. This was followed by a second and subsequent force runs, as MBP was found to undergo time-dependent conformational changes.

QCM-D Experiments. A Quartz Crystal Microbalance with Dissipation (QCM-D E4, Biolin Scientific)[27] was used to measure the mass density of adsorbed MBP. A silicon dioxide (SiO_2) sensor (Biolin Scientific) was used as the substrate since the SiO_2 surface is negatively charged like the myelin sheath. SiO_2 sensors were rinsed with ethanol, followed by exposure to UV-ozone plasma for 30 min before use. The baseline was calibrated by injecting the buffer (mentioned in the Materials section) using a peristaltic pump with a flow rate of Q = 400 μL/min. Based on the information from QSense, Q = 400 μL/min gives a flow velocity of 0.96 m/s, corresponding to a Reynolds number of Re = 9.1, which indicates that the system is in the laminar flow regime (Re < 2300). After the frequency and dissipation values became stable, MBP solution at three different concentrations (25, 10, and 5 μg/mL) was injected simultaneously to three different QCM-D chambers for 1 h. The frequency changes (of the third and fifth harmonics) were converted to surface concentrations using the Sauerbrey equation,[28] which is an excellent approximation for a low-dissipation system ($\Delta D/\Delta f < 10^{-6}/10$ Hz),[29] where ΔD is the dissipation change.

Justification for Using Mica and Silica As Model Surfaces for Cytoplasmic Myelin Lipid Bilayers. The negative surface charge density of cytoplasmic myelin lipid membranes is calculated to be 5.4 nm^2 per unit charge e$^-$ based on the fraction of negatively charged lipids,[15] and was measured to be 7.5 nm^2 per unit charge e$^-$.[30] The model surfaces that we used for this study are mica (for the SFA) and silica (for the QCM-D). The negative surface charge of silica at pH 7.4 and NaCl concentration of 0.15 M is 3−4 nm^2 per unit charge e$^-$,[31] while mica at these conditions has 2−3 nm^2 per unit charge e$^-$.[32] In addition to the similar charge densities for all the surfaces, the rms surface roughness is also similar and less than 1.2 nm. These comparisons indicate that the mica and SiO_2 surfaces used are good model surfaces for cytoplasmic myelin lipid bilayers as far as the charge densities and roughnesses are concerned. The importance of the different fluidities and other properties of the model and biological membrane surfaces remains to be investigated.

Modeling and fitting the QCM-D data. To solve the systems of differential equations and fit the data, MATLAB R2009b was used. Prior to fitting, all the equations were nondimensionalized by normalizing all the variables by characteristic values. The systems of differential equations were numerically solved and fitted to the QCM-D data using a least-squares method. In order to implement the importance of the initial data points (where there is a drastic change in surface concentration with time), a weight parameter was introduced (adding 10 times more weighting to the data points of t < 12 min).

RESULTS AND DISCUSSION

Effects of Bulk MBP Concentration on the Interaction Forces between Mica Surfaces. Figure 2a shows the normalized force (F/R) versus distance (D) curves of MBP at two bulk concentrations (C = 25 and 100 μg/mL) after equilibrating for 3 h. Zero separation distance (D = 0) is defined as mica−mica contact in air. At C = 25 μg/mL, the steric "hard-wall" thickness, D_{Steric}, was 3 nm, similar to the thickness of MBP (σ_{MBP}) in its compact C-shape conformation (see schematic in Figure 2b).[16] On the approach, the steric repulsion due to trapped MBP between the mica surfaces starts around D = 6 nm, which is comparable to $2\sigma_{MBP}$. The measured adhesion force, F_{ad}/R = 1.1 mN/m, which corresponds to adhesion energy of $E_{ad} = F_{ad}/1.5\pi R$ = 0.23 mJ/m^2 using Johnson−Kendall−Roberts (JKR) theory,[33] is slightly smaller compared to a previously measured adhesion force, F_{ad}/R = 1.7 mN/m (E_{ad} = 0.36 mJ/m^2), of MBP between normal (nonpathological) myelin lipid bilayers.[22] During separation from adhesive contact, the MBP molecules were found to stretch 5 nm before adhesive detachment occurred. This length is less than the contour length (15 nm)[16,34] and much less than the fully extended length (50 nm) of MBP.[19]

The force−distance profiles at MBP concentration of C = 100 μg/mL showed the following differences compared to the

DOI: 10.1021/acs.langmuir.5b00145
Langmuir 2015, 31, 3159−3166

profiles at C = 25 μg/mL: (i) the steric repulsion on approach is more pronounced with the repulsion starting at D = 30 nm; (ii) D_{Steric} was equal to 6 nm or $2\sigma_{MBP}$ at F/R = 6 mN/m, indicating a double layer of MBP (see schematic in Figure 2b); (iii) the adhesion force is weaker (F_{ad}/R = 0.7 mN/m, E_{ad} = 0.23 mJ/m^2), and (iv) the surfaces detached at a larger distance (D_j = 18 nm) before they jumped apart, which indicates that the MBP molecules stretch farther than at C = 25 μg/mL (Figure 2b).

These results demonstrate that at low solution concentration of MBP (C = 25 μg/mL), MBP molecules form a more compact monolayer film with a higher adhesion force, while at a high MBP concentration (C = 100 μg/mL), the protein forms a multilayer (gel-like) film with stronger steric repulsion, thicker steric wall thickness, lower adhesion force/energy (due to cohesion between the MBP molecules), and more pronounced stretching of the molecules before the surfaces detach (jump apart in SFA experiments).

Conformational Changes of Adsorbed MBP upon Adsorption. The structure of MBP changes in the presence of lipids;[10] however, it is a slow process that can take several minutes. Figure 3 shows how the force−distance profile changes as MBP is allowed to structurally rearrange on the mica surfaces. The first force runs (black circles) show the force distance profiles 15 min after MBP injection, while subsequent force runs (red circles) were performed after 3 h. After 3 h, no further changes are observed in the force distance profiles, which led to the conclusion that MBP reached its equilibrium conformation. To test for reproducibility, we also performed force runs immediately after the first, which gave the same force profiles as in the first run, and had no effects on the second run after 3 h, which was also obtained if the two surfaces were brought together for the first time after 3 h. Thus, the same force profiles are obtained 3 h after the adsorption irrespective of whether or not the surfaces are previously brought together. These tests show that any long-term changes, e.g., after 3 h, after the adsorption time, are due to "natural" relaxations of the MBP and not due to the "push-pull" effects of previous force runs.

At C = 25 μg/mL, no adhesion (i.e., purely repulsive forces) was measured between the two mica surfaces with a layer of MBP trapped between them after 15 min. However, after 3 h, the adhesion F_{ad}/R increases up to ∼1.1 mN/m (E_{ad} = 0.23 mJ/m^2) even though only minor changes in the steric wall distance, D_{Steric}, were found. The appearance of an adhesive contact indicates that MBP molecules underwent a structural change that favors adhesion between MBP molecules and the mica surface. The positive charges on MBP will conform to the negative mica surface, while the hydrophobic groups of MBP will oppose contact with the hydrophilic mica surface. Also, hydrophobic groups of MBP molecules will attract similar groups on other MBP molecules in close proximity. The two effects of MBP−mica (adhesion) and MBP−MBP (cohesion) interactions that lead to structural changes are modeled later (see below).

At C = 100 μg/mL, MBP molecules formed a thicker layer (D_{Steric} = 10 nm at F/R = 6 mN/m) compared to at 25 μg/mL (D_{Steric} = 3 nm at F/R = 6 mN/m), which became more compact after 3 h (D_{Steric} = 6 nm at F/R = 6 mN/m). On the other hand, significant adhesion (F_{ad}/R = 0.8 mN/m, E_{ad} = 0.17 mJ/m^2) was observed shortly after the injection of MBP, which only slightly increases (to F_{ad}/R = 0.9 mN/m, E_{ad} = 0.19 mJ/m^2) after 3 h. The significant inward shift of the steric hard wall distance indicates a structural change of the MBP film. Furthermore, the cohesive interaction force seems to be independent of conformation or protein layer thickness.

QCM-D measurements provided further detailed information on the MBP adsorption mechanism and its associated structural changes. Figure 4 shows plots of surface concentration (C_θ, obtained by the Sauerbrey equation[28]) of MBP on an SiO_2 surface as a function of the adsorption time (t). At C = 25 μg/mL, the surface concentration of MBP, C_θ, increased rapidly and peaked at 450 ng/cm^2 at t = 90 s after injection of the MBP solution, and then settled to C_θ = 320 ng/cm^2 after t = 15 min (900 s). The rate of surface coverage after injection of MBP solution decreases with decreasing concentrations, and the initial overshoot of surface coverage also decreases with decreasing concentration and was nonexistent at concentrations below C = 5 μg/mL (see inset, Figure 4). At C = 10 μg/mL, the C_θ reached a peak value of 355 ng/cm^2 after t = 4 min, which equilibrated to C_θ = 305 ng/cm^2 after t = 30 min. At C = 5 μg/mL, no peak was observed, and C_θ slowly increased to an equilibrium value of C_θ = 305 ng/cm^2.

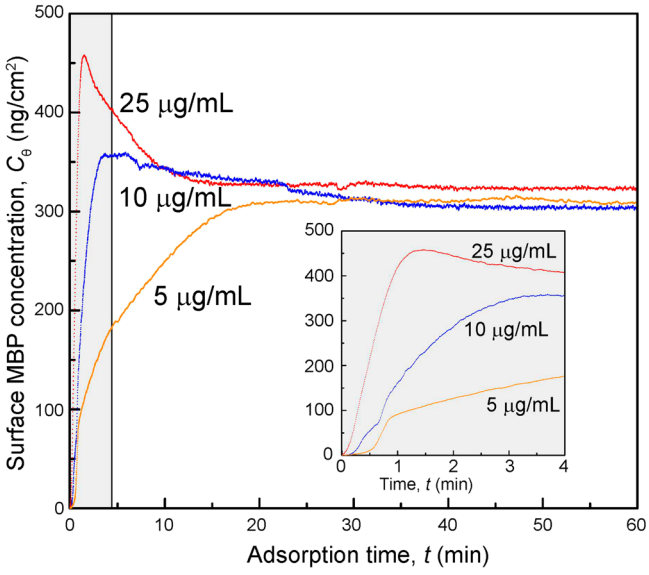

Figure 4. Surface MBP concentration curves as a function of adsorption time showing the adsorption of MBP on the SiO_2 surfaces using a QCM-D. The plots were generated by applying the Sauerbrey equation on the QCM-D data collected from third and fifth harmonics.

It is interesting to note that, regardless of the bulk MBP concentration, C, the surface concentration equilibrated to similar values (C_θ = 310 ± 10 ng/cm^2) after 30 min. Together with the dissipation data measured with QCM-D (Figure 5), these results suggest that MBP molecules form a weakly bound and soft preadsorbed layer on an SiO_2 surface, followed by conformational changes to a more compact (and thinner) and more stable structure (see the inset schematic in Figure 5) that occupies a larger area per molecule. The results also agree with the SFA results (see Figure 3b), which showed an initial thick layer that equilibrates into a more compact layer after 3 h.

Modeling the MBP Adsorption Mechanism. Based on the SFA and QCM-D results, we propose a "three-step model" (see Figure 6a) for the MBP adsorption mechanism: (i) Bulk MBP moves from the bulk, across the concentration boundary layer, to the "subsurface" (bulk region in close proximity to the silica surface); (ii) MBP molecules from the subsurface adsorb

DOI: 10.1021/acs.langmuir.5b00145
Langmuir 2015, 31, 3159−3166

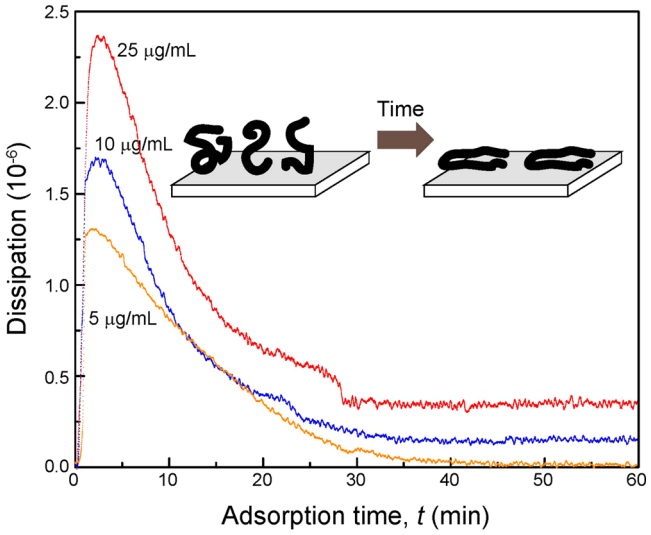

Figure 5. Dissipation of adsorbed MBP on silica measured by a QCM-D. The dissipation values rapidly increase shortly after injection of MBP solution (t < 5 min) and gradually plateau to a lower value after t > 30 min. These skewed curves indicate conformational changes of MBP from a soft structure to a stiffer structure after adsorption.

to the surface, and (iii) the adsorbed MBP molecules undergo a conformational change. This model can be expressed using the following equation:

$$\mathbf{A} \overset{k_m}{\leftrightarrow} \mathbf{B} \underset{k_{-1}}{\overset{k_1}{\rightleftarrows}} \mathbf{C} \overset{k_2}{\rightarrow} \mathbf{D} \quad (1)$$

where, **A**, **B**, **C**, and **D** represent MBP in the bulk, subsurface MBP, adsorbed MBP, and adsorbed MBP after a conformational change, respectively. Here, k_m is the mass transfer coefficient for the diffusion of MBP across the boundary layer, k_1 is the rate constant for the adsorption of MBP from the subsurface to the surface, k_{-1} is the rate constant for desorption of the adsorbed MBP, and k_2 is the rate constant for the conformational change of adsorbed MBP. For simplifying the model, we assume that (i) the concentration boundary layer is at steady state (this is justified in Supporting Information section SI#1); (ii) the adsorbed MBP molecules can either detach or change their conformation; (iii) the conformational change of MBP on the surface is irreversible, and (iv) after the conformational change (state **C** to **D**), MBP is strongly bound to the surface and does not detach to the subsurface.

The MBP adsorption onto a silica surface was measured by a QCM-D at three different bulk concentrations of MBP, C_{A0} = 25, 10, and 5 μg/mL (Figure 4 and 6b–d). These three solutions were guided into the QCM-D chamber (volume = 40 μL and prefilled with buffer solution) at a constant volumetric flow rate of Q = 400 μL/min. The chamber concentration of MBP, C_A, increases from 0 (pure buffer) to C_{A0} after a residence time τ, which is 0.1 min; therefore, data below time scales of this order was ignored when fitting data to the model.

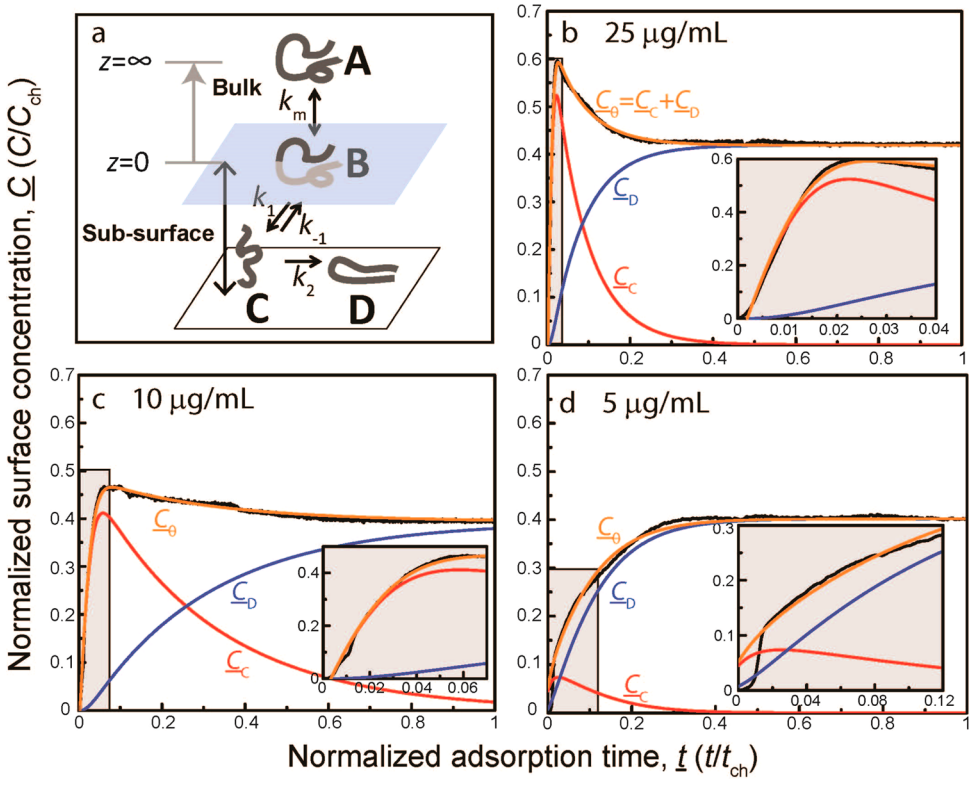

Figure 6. (a) The proposed 3-step model of the MBP adsorption mechanism and their fit on the surface concentration data from Figure 4, at three difference bulk concentrations (b) 25, (c) 10, and (d) 5 μg/mL. The surface concentration data are normalized by a characteristic time (t_{ch} = 60 min) and concentration (C_{ch} = 768.3 ng/cm^2). The normalized surface concentration measured by the QCM-D (black) was fitted to the model (orange). The plots also show the model data of surface concentration of the adsorbed MBP (red, state **C**) and the surface concentration of the structurally conformed MBP (blue, state **D**).

DOI: 10.1021/acs.langmuir.5b00145
Langmuir 2015, 31, 3159–3166

The rate of transfer of MBP across the boundary layer (from state **A** to **B** in eq 1) can be modeled using the standard mass transport relationship:[35]

$$J_A = k_m(C_{A0} - C_B) \tag{2}$$

where C_B is the bulk concentration of MBP at the subsurface. The MBP can go from the subsurface to an adsorbed state (state **C** in eq 1) at the surface. The net adsorption rate of adsorbed MBP, dC_C/dt, is directly proportional to the subsurface MBP concentration (C_B) and θ_f, the fraction of vacant sites at the silica surface, given by the following equation:

$$\theta_f = 1 - \frac{C_C}{C_{Csat}} - \frac{C_D}{C_{Dsat}} \tag{3}$$

Here, C_D is the MBP concentration after the conformational change, and C_{Csat} and C_{Dsat} are the saturated surface concentrations of MBP when it completely covers the surface with initially adsorbed MBP only or with conformationally changed MBP only, respectively. To calculate C_{Csat}, we approximate the adsorbed form of MBP (MBP in state **C**) using prolate ellipsoidal geometry.[5] Assuming a hydrodynamic area of 400 Å^2/molecule of the adsorbed MBP in state **C**, we calculate a complete coverage of C_{Csat} = 768.3 ng/cm^2. The complete coverage of conformationally-changed MBP at the silica surface, C_{Dsat}, is equal to the final surface concentration of MBP molecules found from the QCM-D measurements (see Figure 4). After a sufficiently long time has elapsed (t > 60 min), the QCM-D data of all concentrations of MBP approach the same value of C_{Dsat} = 304 ng/cm^2, where the silica surface is completely covered with MBP molecules in their final stable structure.

A balance of the MBP molecules at the subsurface yields (see eq 1):

$$\underset{\text{Transport of MBP from bulk to subsurface}}{k_m(C_{A0} - C_B)} = \underset{\text{Consumption of subsurface MBP by adsorption to C}}{k_1\theta_f C_B} - \underset{\text{Production of subsurface MBP by desorption of C}}{k_{-1}C_C} \tag{4}$$

This provides the following expression for the subsurface MBP concentration, C_B:

$$C_B = \frac{k_m C_{A0} + k_{-1}C_C}{k_m + k_1\theta_f} \tag{5}$$

The rate of adsorbed MBP in state **C** can be expressed as the following Langmuir-type differential equation (see eq 1):

$$\frac{dC_C}{dt} = k_1 C_B\theta_f - k_{-1}C_C - k_2 C_C \tag{6}$$

Using eq 5, the above equation can be simplified to

$$\frac{dC_C}{dt} = k_m\left(\frac{k_1\theta_f C_{A0} - k_{-1}C_C}{k_m + k_1\theta_f}\right) - k_2 C_C \tag{7}$$

The rate of the MBP conformation change at the silica surface can be expressed by the following, simple kinetic equation (see eq 1):

$$\frac{dC_D}{dt} = k_2 C_C \tag{8}$$

The total surface concentration, C_θ, measured from the QCM-D, is the sum of C_C and C_D:

$$C_\theta = C_C + C_D \tag{9}$$

Table 1 summarizes the overall equations and units for the proposed three-step adsorption model given in eqs 3 and 7−9,

Table 1. Equations for the Proposed Three-Step Model

Equations
$\frac{dC_C}{dt} = k_m\left(\frac{k_1\theta_f C_{A0} - k_{-1}C_C}{k_m + k_1\theta_f}\right) - k_2 C_C$ (7)
$\frac{dC_D}{dt} = k_2 C_C$ (8)
$C_\theta = C_C + C_D$ (9)
$\theta_f = 1 - \frac{C_C}{C_{Csat}} - \frac{C_D}{C_{Dsat}}$ (3)
Units
C_A, C_{A0}, C_B: ng/cm^3
C_C, C_D, C_{Csat}, C_{Dsat}, C_θ: ng/cm^2
k_{-1}, k_2: min^{-1}
k_m, k_1: cm·min^{-1}
t, τ: min

together with the units for each variable. For convenience of modeling and fitting, the QCM-D data, as well as all of the variables, were normalized (see SI #2 for the normalized equations and dimensionless parameters) by the characteristic time (t_{ch} = 60 min) and concentration ($C_{ch} = C_{Csat}$ = 768.3 ng/cm^2). The normalized variables are underlined.

Figure 6b−d shows the normalized QCM-D data (same data as in Figure 4) together with the values of the normalized MBP surface concentrations ($\underline{C}_\theta = \underline{C}_C + \underline{C}_D$) that are fitted to the three-step adsorption model. Table 2 shows the fitting

Table 2. Parameters for the Fits in Figure 6

concentration (μg/mL)	k_m	k_1/k_{-1}	k_2
25	0.0259	0.0457	0.135
10	0.0244	0.0719	0.0461
5	0.0192	0.0222	0.570

parameters used in Figure 6b−d obtained by a weighted, least-squares fit of predictions of C_θ from the model to the experimental data in MATLAB. The differential equations were integrated using the *ode23s* routine for stiff ordinary differential equations, and the minimization of the residual was accomplished using the *fmincon* routine with default functional and variable tolerances. As can be seen in Figure 6, the proposed model shows excellent agreement with the experimental data. Note that we have only reported the ratio, k_1/k_{-1}, rather than the individual values of these rate constants. This is because, during the fitting process, we discovered that the adsorption rate of MBP (state **B** to state **C**) in our QCM-D experiments is controlled by mass transfer limitations. Equation 5 suggests that mass-transfer-limited adsorption occurs when $k_m \ll k_1\theta_f$, for which the governing equation for C_C (eq 7) reduces to

$$\frac{dC_C}{dt} = k_m\left(C_{A0} - \frac{k_{-1}}{k_1}\frac{C_C}{\theta_f}\right) - k_2 C_C \tag{10}$$

The above equation suggests that the dynamics of C_C does not depend separately on k_1 and k_{-1}, but only on the ratio $k_1/$

DOI: 10.1021/acs.langmuir.5b00145
Langmuir 2015, 31, 3159−3166

k_{-1}. This was experienced during the fitting process; the residual and the agreement between theory and experiment were relatively insensitive to the individual values of k_1 and k_{-1} as long as their ratio was close to the optimum value. The mean mass transfer coefficient in the three experiments is 0.023 cm/min. Since k_1 has to exceed k_m to be in the mass-transfer-dominated limit, 0.023 cm/min represents an approximate lower bound for the rate constant k_1 in the experiments, and the corresponding, approximate lower bounds for k_{-1} for the three bulk MBP concentrations, 25 μg/mL, 10 μg/mL and 5 μg/mL, are 0.503 min^{-1}, 0.320 min^{-1} and 1.04 min^{-1}, respectively.

CONCLUSIONS

Direct measurements using an SFA and QCM-D provide quantitative and qualitative information about the buildup of MBP layers and the bridging adhesion forces of MBP, and the kinetics of MBP adsorption to surfaces and the conformational changes of MBP with time (energies). The bridging forces (energies) and the thickness of the MBP monolayer between two mica surfaces are F_{ad}/R = 1.0 ± 0.1 mN/m (E_{ad} = 0.21 ± 0.02 mJ/m^2) and D_{Steric} = 3 nm, respectively (at a bulk concentration of C = 10 mg/mL and 3 h after injection of MBP).

On silica surfaces, the final equilibrium structure of MBP occupies 310 ± 10 ng/cm^2 on a silica surface. Covering a bare silica surface with MBP molecules at equilibrium takes 30 min. The adsorption of MBP on a SiO_2 surface can best be described by a three-step adsorption model, where bulk MBP diffuses across the concentration boundary layer, adsorbs to the SiO_2 surface, and undergoes a slow, conformational change to a stable and adhesive structure. The derived adsorption model can be used to fit the adsorption kinetics of a wide range of intrinsically disordered proteins and perhaps extended further to the adsorption of various chemical compounds, which undergo chemical reactions or conformational changes after adsorbing to surfaces.

This study was performed on model solid substrates, rather than on and between myelin lipid bilayers. Therefore, we are likely ignoring some important effects that would be present in naturally-occurring lipid bilayers, such as lipid−protein coupling, hydrophobic interactions between lipids and proteins, undulation of lipid bilayers, and effects from lipid domains. Nevertheless, this study still provides qualitative information on MBP adsorption and bridging mechanisms to negatively charged SiO_2 and mica surfaces, resembling charged myelin lipid bilayers.

ASSOCIATED CONTENT

Supporting Information

Estimation of boundary layer thickness and time for boundary layer development, non-dimensionalized equations with fitting parameters, and raw QCM data. This material is available free of charge via the Internet at http://pubs.acs.org.

AUTHOR INFORMATION

Corresponding Author

*E-mail: Jacob@engineering.ucsb.edu; Phone: (805) 893-8407; Fax: (805) 893-7870.

Notes

The authors declare no competing financial interest.

ACKNOWLEDGMENTS

This research was supported by the National Institutes of Health under Award Number R01 GM076709 and the National Science Foundation under Award Number CHE-1059108 (D.W.L., K.K., and J.N.I.), and the Canadian Insitutes of Health Research (MOP 86483) (J.M.B.). A.R. acknowledges support from National Science and Engineering Research Council under the Discovery Grant # 402005. We also thank Dr. Matthew Dixon, Dr. Elizabeth Schneider, and Professor Malkiat Johal for supporting the QCM-D experiment.

REFERENCES

(1) Deber, C. M.; Reynolds, S. J. Central nervous system myelin: Structure, function, and pathology. *Clin. Biochem.* **1991**, *24* (2), 113−134.
(2) Kirschner, D. A.; Inouye, H.; Ganser, A. L.; Mann, V. Myelin membrane-structure and composition correlated - A phylogenetic study. *J. Neurochem.* **1989**, *53* (5), 1599−1609.
(3) Smith, R. The basic-protein of CNS myelin: Its structure and ligand-binding. *J. Neurochem.* **1992**, *59* (5), 1589−1608.
(4) Inouye, H.; Kirschner, D. A. Membrane interactions in nerve myelin. 1. Determination of surface-charge from effects of pH and ionic-strength on period. *Biophys. J.* **1988**, *53* (2), 235−245.
(5) Martenson, R. *Myelin: Biology and Chemistry*; CRC Press: Boca Raton, FL, 1992.
(6) Morell, P. *Myelin*, 2 ed.; Plenum Press: New York, 1984.
(7) Genain, C. P.; Cannella, B.; Hauser, S. L.; Raine, C. S. Identification of autoantibodies associated with myelin damage in multiple sclerosis. *Nat. Med.* **1999**, *5* (2), 170−175.
(8) Hafler, D. A. Multiple sclerosis. *J. Clin. Invest.* **2004**, *113* (6), 788−794.
(9) Ohler, B.; Graf, K.; Bragg, R.; Lemons, T.; Coe, R.; Genain, C.; Israelachvili, J.; Husted, C. Role of lipid interactions in autoimmune demyelination. *Biochim. Biophys. Acta, Mol. Basis Dis.* **2004**, *1688* (1), 10−17.
(10) Harauz, G.; Ishiyama, N.; Hill, C. M. D.; Bates, I. R.; Libich, D. S.; Fares, C. Myelin basic protein: Diverse conformational states of an intrinsically unstructured protein and its roles in myelin assembly and multiple sclerosis. *Micron* **2004**, *35* (7), 503−542.
(11) Hill, C. M.; Bates, I. R.; White, G. F.; Hallett, F. R.; Harauz, G. Effects of the osmolyte trimethylamine-*N*-oxide on conformation, self-association, and two-dimensional crystallization of myelin basic protein. *J. Struct. Biol.* **2002**, *139* (1), 13−26.
(12) Hill, C. M. D.; Haines, J. D.; Antler, C. E.; Bates, I. R.; Libich, D. S.; Harauz, G. Terminal deletion mutants of myelin basic protein: New insights into self-association and phospholipid interactions. *Micron* **2003**, *34* (1), 25−37.
(13) Sedzik, J.; Kirschner, D. A. Is myelin basic-protein crystallizable? *Neurochem. Res.* **1992**, *17* (2), 157−166.
(14) Boggs, J. M. Myelin basic protein: A multifunctional protein. *Cell. Mol. Life Sci.* **2006**, *63* (17), 1945−1961.
(15) Min, Y.; Kristiansen, K.; Boggs, J. M.; Husted, C.; Zasadzinski, J.; Israelachvili, J. N. Interaction forces and adhesion of supported myelin lipid bilayers modulated by myelin basic protein. *Proc. Natl. Acad. Sci. U.S.A.* **2009**, *106*, 3154−3159.
(16) Beniac, D. R.; Luckevich, M. D.; Czarnota, G. J.; Tompkins, T. A.; Ridsdale, R. A.; Ottensmeyer, F. P.; Moscarello, M. A.; Harauz, G. Three-dimensional structure of myelin basic protein. 1. Reconstruction via angular reconstitution of randomly oriented single particles. *J. Biol. Chem.* **1997**, *272* (7), 4261−4268.
(17) Jo, E. J.; Boggs, J. M. Aggregation of acidic lipid vesicles by myelin basic protein: Dependence on potassium concentration. *Biochemistry* **1995**, *34* (41), 13705−13716.
(18) Macnaughtan, W.; Snook, K. A.; Caspi, E.; Franks, N. P. An X-ray-diffraction analysis of oriented lipid multilayers containing basic-proteins. *Biochim. Biophys. Acta* **1985**, *818* (2), 132−148.

DOI: 10.1021/acs.langmuir.5b00145
Langmuir 2015, 31, 3159−3166

(19) Mueller, H.; Butt, H. J.; Bamberg, E. Force measurements on myelin basic protein adsorbed to mica and lipid bilayer surfaces done with the atomic force microscope. *Biophys. J.* **1999**, *76* (2), 1072−1079.
(20) Wheeler, D.; Bandaru, V. V. R.; Calabresi, P. A.; Nath, A.; Haughey, N. J. A defect of sphingolipid metabolism modifies the properties of normal appearing white matter in multiple sclerosis. *Brain* **2008**, *131*, 3092−3102.
(21) Lee, D. W.; Min, Y. J.; Dhar, P.; Ramachandran, A.; Israelachvili, J. N.; Zasadzinski, J. A. Relating domain size distribution to line tension and molecular dipole density in model cytoplasmic myelin lipid monolayers. *Proc. Natl. Acad. Sci. U.S.A.* **2011**, *108* (23), 9425−9430.
(22) Lee, D. W.; Banquy, X.; Kristiansen, K.; Kaufman, Y.; Boggs, J. M.; Israelachvili, J. N. Lipid domains control myelin basic protein adsorption and membrane interactions between model myelin lipid bilayers. *Proc. Natl. Acad. Sci. U.S.A.* **2014**, *111* (8), E768−E775.
(23) Ahmed, M. A. M.; Bamm, V. V.; Harauz, G.; Ladizhansky, V. Solid-State NMR Spectroscopy of Membrane-Associated Myelin Basic Protein-Conformation and Dynamics of an Immunodominant Epitope. *Biophys. J.* **2010**, *99* (4), 1247−1255.
(24) Cheifetz, S.; Moscarello, M. A. Effect of bovine basic-protein charge microheterogeneity on protein-induced aggregation of unilamellar vesicles containing a mixture of acidic and neutral phospholipids. *Biochemistry* **1985**, *24* (8), 1909−1914.
(25) Israelachvili, J.; Min, Y.; Akbulut, M.; Alig, A.; Carver, G.; Greene, W.; Kristiansen, K.; Meyer, E.; Pesika, N.; Rosenberg, K.; Zeng, H. Recent advances in the surface forces apparatus (SFA) technique. *Rep. Prog. Phys.* **2010**, *73* (3), 036601.
(26) Israelachvili, J. Thin-film studies using multiple-beam interferometry. *J. Colloid Interface Sci.* **1973**, *44* (2), 259−272.
(27) Dixon, M. C. Quartz crystal microbalance with dissipation monitoring: Enabling real-time characterization of biological materials and their interactions. *J. Biomol. Tech.: JBT* **2008**, *19* (3), 151−8.
(28) Sauerbrey, G. Verwendung von schwingquarzen zur wagung dunner schichten und zur mikrowagung. *Z. Phys.* **1959**, *155* (2), 206−222.
(29) Voinova, M. V.; Rodahl, M.; Jonson, M.; Kasemo, B. Viscoelastic acoustic response of layered polymer films at fluid-solid interfaces: Continuum mechanics approach. *Phys. Scr.* **1999**, *59* (5), 391−396.
(30) Banquy, X.; Kristiansen, K.; Lee, D. W.; Israelachvili, J. N. Adhesion and hemifusion of cytoplasmic myelin lipid membranes are highly dependent on the lipid composition. *Biochim. Biophys. Acta, Biomembr.* **2012**, *1818* (3), 402−410.
(31) Iler, R. K. *The Chemistry of Silica*; John Wiley & Sons: New York, 1979.
(32) Israelachvili, J. N. *Intermolecular and Surface Forces*, 3rd ed.; Academic Press: London, 2011.
(33) Johnson, K. L.; Kendall, K.; Roberts, A. D. Surface energy and contact of elastic solids. *Proc. R. Soc., London Ser. A: Math. Phys. Sci.* **1971**, *324* (1558), 301−313.
(34) Epand, R. M.; Moscarel, M.; Zierenbe, B.; Vail, W. J. Folded conformation of encephalitogenic protein of human brain. *Biochemistry* **1974**, *13* (6), 1264−1267.
(35) Leal, L. G. *Advanced Transport Phenomena: Fluid Mechanics and Convective Transport Processes*; Cambridge University Press: New York, 2007.

DOI: 10.1021/acs.langmuir.5b00145
Langmuir 2015, 31, 3159−3166